DRAFT

Final Report Certification
for
CRADA Number ORNL 99-0549
Between
UT-Battelle, LLC
and
The Timken Company
(Participant)

Instructions:

Mark the appropriate statement in 1a or 1b below with an 'IX." Refer to the articles in the CRADA terms and conditions governing the identification and marking of Protected CRADA Information.

If no PCI is identified, the report will be distributed without restriction. If PCI is identified, the report distribution will be limited in accordance with the CRADA terms and conditions governing release of data. In all cases items 2 and 3 must be true. That is, the report cannot

contain Proprietary Information and a disclosure must be filed prior to release of the report. This certification may either be made by using this form or may be made on company letterhead if the Participant desires. A faxed copy of this completed form is acceptable.

The following certification is made for the subject final report:

1. (a) IX The final report contains information that qualifies as "Protected CRADA Information" (PCI). The PCI legend is printed on the report cover, and the PCI is clearly identified.

OR

(b) The final report does not contain "Protected CRADA Information." The "Approved for Public Release" legend is printed on the report cover. 2. The final report does not contain Proprietary Information. 3. By the signature below, the Participant has no objection to the public distribution of the final report due to patentable information.

For the Participant:

Robert V. Kolarik II
(Name)

Project Manager - Process Technology
(Title)

10/22/02
(Date)

DRAFT

C/ORNL99-0549

CRADA Final Report
for
CRADA Number ORNL 99-0549

DEVELOPMENT OF AVERSITILE LASER ULTRASONIC SYSTEM AND APPLICATION TO ON-LINE MEASUREMENT FOR PROCESS CONTROL OF WALL THICKNESS AND ECCENTRICITY OF STEEL SEAMLESS MECHANICAL TUBING

R. A. Kisner, S. W. Kercel, B. Damiano
P. R. Bingham, T. F. Gee, R. W. Tucker
M. R. Moore, Mike Hileman, Mike Emery
Roberto Lenarduzzi, J. E. Hardy, Ken Weaver,
and Richard Crutcher
Oak Ridge National Laboratory

R. V. Kolarik, II and R. H. Vandervaart
The Timken Company

Prepared by the
Oak Ridge National Laboratory
Oak Ridge, Tennessee 37831
managed by
UT-Battelle, LLC
for the
U.S. Department of Energy
Under contract DE-AC05-00OR22725

Abstract

Researchers at the Timken Company conceived a project to develop an on-line instrument for wall thickness measurement of steel seamless mechanical tubing based on laser ultrasonic technology. The instrument, which has been installed and tested at a piercing mill, provides data on tube eccentricity and concentricity. Such measurements permit fine-tuning of manufacturing processes to eliminate excess material in the tube wall and therefore provide a more precisely dimensioned product for their customers. The resulting process energy savings are substantial, as is lowered environmental burden. The expected savings are $85.8 million per year in seamless mechanical tube piercing alone. Applied across the industry, this measurement has a potential of reducing energy consumption by $6x10^{12}$ BTU per year, greenhouse gas emissions by 0.3 million metric tons carbon equivalent per year, and toxic waste by 0.255 million pounds per year.

The principal technical contributors to the project were the Timken Company, Industrial Materials Institute (IMI, a contractor to Timken), and Oak Ridge National Laboratory (ORNL). Timken provided mill access as well as process and metallurgical understanding. Timken researchers had previously developed fundamental ultrasonice analysis methods on which this project is based. IMI developed and fabricated the laser ultrasonic generation and receiver systems. ORNL developed Bayesian and wavelet based real-time signal processing, spread-spectrum wireless communication, and explored feature extraction and pattern recognition methods. The resulting instrument has successfully measured production tubes at one of Timken's piercing mills.

This report concentrates on ORNL's contribution through the CRADA mechanism. The three components of ORNL's contribution were met with mixed success. The real-time signal-processing task accomplished its goal of improvement in detecting time of flight information with a minimum of false data. The signal processing algorithm development resulted in a combination of processing steps that can be set to generate no spoofs from noise, while simultaneously missing fewer than 10% of good trials. The algorithm leads to a 95% probability that the estimate of time of flight is good to within 4 time bins or fewer for laser excitations above 30 mJ for the first two echoes of the signal. Receiver Operating Characteristic (ROC) curves for the algorithm indicate that the algorithm is very robust against errors for excitations above at 35 mJ and above, tolerable at 30 mJ and unacceptable below 30 mJ.

For the wireless tube detection task, a 916.4 MHz spread spectrum transmitter, repeater, receiver system was developed based on previous wireless research at ORNL. The wireless detector identified when a hot tube or billet entered the piercing process and signaled the laser systems to get ready for a measurement. At the first of the installation, we saw slight microwave interference from a nearby nationwide pager system, which we corrected by moving the center frequency of our direct sequence, spread spectrum transmitter. We determined that exposure to the harsh environments of the steel mill over long duration did not seem to adversely effect the equipment. However, we continued to see glitches in the digital portion of the data processing, which seemed to originate from the handshake between the IMI computer and the ORNL receiver. The continuous poling

of the main control computer causes a buffer overrun and results in a frequency shift. This problem and a second one that involved intermittent start-up delays were not identified as potential follow on work.

The feature extraction and pattern recognition task was a challenge technically and programmatically. Delays in the laser system startup owing to the complex nature of the instrument being developed postponed data collection for this task. Because of unexpected laser system problems, the pattern recognition task was reduced and eventually stopped so funds could be redirected to IMI to make corrections to the generation laser optics. Most of the feature extraction task could not be performed because sufficient useful data were not available.

However, even with the sparse data set collected and the work stoppage, the limited studies have provided useful information. Two items in particular are worth highlighting. First of all, although some of the more obvious patterns are visible in the raw LUT thickness graphs, bandpass filtering and/or averaging of these graphs can help isolate certain features such as low frequency thickness variations. Further study needs to be done with frequency filtering. In fact, filtering the raw data in certain frequency bands would likely help the mill operators identify certain mill conditions more easily. Second, the 2-dimensional thickness plots could be useful in helping operators discover unknown mill conditions that affect the tube as seen by the barber pole pattern in the 2-D maps.

The project has shown that the system elements necessary to accomplish the measurement as devised can be accommplished in a mill setting, which is subject to dirt, water spray, temperature extremes and vibration. Ultrasound can be induced into hot stell tubing using fiber-coupled laser light and the return echo detected using laser-based interferometry. The location of the measurement can be determined using laser Doppler velocimetry and the temperature determined with fiberized pyrometry.

Statement of the Objectives

The purpose of the Cooperative Research and Development Agreement CRADA between Oak Ridge National Laboratory (ORNL) and Timken was to develop and demonstrate a laser-based ultrasonic (LBU) system. The LBU system's purpose was to, online and by non-contact means, measure wall thickness and eccentricity of hot steel seamless mechanical tubing as it is being processed in a piercing mill. The project's goal was to build a cost-effective, modular system that could be easily upgraded or relocated. The project also aimed to transition the technology into an industrial environment to demonstrate the long-term utility of the technology. Timken and their contractors were responsible for the development of the laser systems, coordinate measurement system, optical detection systems, the development and preparation of the plant operator interface, and the preparation of much of the documentation as well as overall project management.

ORNL's portion of the project consisted of three main tasks: (1) reduce measurement uncertainty by developing software algorithms to enhance the signal-to-noise ratio of the laser interferometer receiver's output; (2) fabricate a wireless detector to indicate that a

tube has entered the tube making process; and (3) increase product yield by developing technology to extract parameters and patterns from the LBU system, the coordinate measurement system, and the temperature measurement system that would indicate "good" or "bad" tubes. The pattern recognition technology can also be used to determine where process wear or other process problems are affecting the tubes.

Benefits to the Funding DOE Office's Mission

The LBU system offers benefits in increased energy efficiency and in the reduction of waste products and environmental concerns. These benefits directly match the mission of DOE. Assumptions and details of the expected energy savings and waste reduction are presented in this section.

Assumptions and detailed calculations of energy savings.

An energy savings of at least $6x10^{12}$ BTU per year would be realized if LBU technology were applied throughout the US steel seamless tube and seamless pipe industry. This is a conservative estimate in that it does not take into account the fact that LBU is also applicable to other processes such as the production of strip and sheet. In tons produced, steel seamless mechanical tube piercing constitutes approximately 0.5% of the total production of entire US steel industry. The industry produced 95 million tons in 1994.[1] Assuming a 1.1% annual rate of growth[2], it is estimated that the present production rate is approximately 100 million tons nationwide. Of this, approximately a half million tons are steel seamless mechanical tube. [3]

How much energy does it take to produce a ton of steel? A rough estimate can be made by comparing the total US production in 1994, 95 million tons [1], and the total energy consumption of the US steel industry in 1994, 2.06 quads, or $2.06x10^{15}$ BTU.[4] Dividing these numbers results in 21.7 million BTU/ton as an average energy consumption. The industry average cost of energy is about 15% of total production cost.[1]

Energy savings in the mechanical tube piercing process are estimated as follows. Comparing its annual production to its annual gas and electric consumption for a typical piercing mill, Timken estimates that it requires 6.30 million BTU in gas, and 0.24 million BTU in electricity to produce a ton of mechanical tubing. Thus, the total energy used in a piercing mill to produce a ton of steel mechanical tubing is approximately 6.54 million BTU (about 96.3% in gas and 3.7% in electricity. Approximately a half million tons of steel are produced per year nationwide in US steel seamless mechanical tube mills.[1] Therefore, the energy required for this production is $3.27x10^{12}$ BTU per year. Timken expects that on-line LBU will reduce the energy costs in its tube mills by 30%. Assuming that this could be applied to tube production across the entire US steel seamless mechanical tube industry, the total energy savings in the piercing process would be $0.981x10^{12}$ BTU, or approximately 0.001 quad.

The energy savings are even greater if the LBU system were applied in related areas of the steel industry. In a typical year, the production of mechanical tubing constitutes

approximately one sixth of total seamless tube and pipe production in the US.[1] There is no fundamental reason why the LBU system to be demonstrated at Timken would not work equally well throughout the US steel seamless tube and pipe industry. Thus, the total energy saved due to the use of on-line thickness and eccentricity measurements in the US steel seamless tube and pipe industry is estimated to be $6x10^{12}$ BTU, or 0.006 quad, per year. It is reasonable to assume that the energy savings across the industry are in the same proportions as energy consumption in the tube piercing industry (about 96.3% in gas, and 3.7% in electricity). Steel-industry-wide the savings estimate is conservative, since it ignores the fact that several other processes in steel making, such as the manufacture of sheet, strip and plate could use and realize similar benefits from LBU thickness measurements.

• Assumptions and detailed calculations of environmental benefits

Widespread adoption of LBU in the steel industry would have considerable environmental benefits. It has the potential of reducing the release of greenhouse gases by 0.3 million metric tons carbon equivalent per year. Similarly, on an industry-wide basis, LBU could reduce the release of toxic waste by 0.255 million pounds per year. Finally, it will substantially reduce other emissions.

• *Greenhouse Gas Emissions*

The reduction in greenhouse gas emissions due to the application of LBU in the steel industry can be estimated from the energy it will save. As already noted, LBU were applied wherever usable throughout the steel seamless tube and pipe industry, the energy savings would be about 0.006 quad per year, with approximately 0.0058 quad from natural gas, and 0.0002 quad from coal-fired electricity. (Note: Most steel production is in the middle west, and the electricity is typically generated from coal.) The carbon coefficient is for natural gas is 14.47 million metric tons per quad, and for coal fired utilities is 25.7 million metric tons per quad.[5] Thus, the annual reduction in carbon from natural gas savings is 0.084 million metric tons, with another 0.005 million metric tons due to savings in electricity. If so, the reduction in CO_2 is conservatively projected at 0.089 million metric tons carbon equivalent per year.
In addition, the steel industry releases 50 million metric tons of carbon in the form of CH_4, and the equivalent of 20 million metric tons of carbon in the form of N_2O. [6] Assume that LBU were applied throughout the steel seamless tube and pipe industry, and led to a 0.3% reduction in the levels of these greenhouse gases (corresponding to an overall 0.3% reduction in energy consumption for the entire US iron and steel industry as calculated previously). If so, the reduction in non-CO_2 greenhouse gases is conservatively projected at 0.21 million metric tons carbon equivalent per year.

How realistic is the total estimate of 0.3 million metric tons reduction carbon equivalent per year? DOE considers it desirable to decrease greenhouse gas emissions in the steel industry by 1.6 to 3.4 million metric tons carbon equivalent by 2010. [7] Taking the high end of the estimate, and assuming 6% of the reduction in greenhouse emissions (corresponding to 6% of the reduction in energy consumption as calculated previously) is attributable to LBU, this would be a total of approximately 0.2 million metric tons carbon equivalent, not far from the estimate of 0.3 million metric tons derived from a completely

different argument. Thus, there is a credible potential that LBU could reduce greenhouse gas emissions in the steel industry by 0.3 million metric tons carbon equivalent per year.

- ***Toxic waste Emissions***

The US iron and steel industry releases 85 million pounds of toxic waste per year, and this includes approximately 150 different toxic compounds.[8] If LBU were applied throughout the steel seamless tube and pipe industry, and productivity gains led to a 0.3% reduction in overall US steel industry pollution levels (corresponding to an overall 0.3% reduction in energy consumption for the entire US iron and steel industry as calculated previously). then the release of toxic waste would be reduced by 0.255 million pounds per year.

- ***Other Effluents***

Other effluents of the steel that will be reduced by increased productivity include slag, dust, sludge and mill scale. [9] It is estimated that 1500-6000 gallons of cooling water are required, and 10-80 pounds of mill scale and 4-60 pounds of sludge are produced for each ton of steel. [10] If LBU improves the productivity of pipe and tube production by 30%, it is reasonable to expect that water consumption is reduced by 25%, and waste products are reduced by 10%. Given a total US seamless steel tube and pipe production of 3-million tons per year, and using the low end of the effluent estimates, cooling water consumption would be reduced by 1125 million gallons per year. Mill scale production would be reduced by 3,000,000 pounds per year. Sludge production would be reduced by 1.2 million pounds per year. Reduction in sludge is especially important, since it can include cadmium, chromium, lead, oil, grease, and machine grindings. [11]

The following quantities of gases (in short tons) are released every year by the steel industry: CO: 1,518,642; NO_2: 138,985; particulate matter of 10 microns or less: 42,368; total particulates: 83,107; SO_2: 238,268; volatile organic compounds: 82,292. [12] Assuming that 3% of these volumes is attributed to seamless tube and pipe production, and that the improved productivity enabled by LBU reduces these emissions by 10%, then the use of LBU would cause the following annual reductions (in short tons) in polluting gases: CO: 4556; NO_2 : 416; particulate matter of 10 microns or less: 127; total particulates: 250; SO_2 : 715; volatile organic compounds: 247.

There are four areas in which steel production should be improved.[13,14] LBU addresses three areas. It improves process efficiency by producing fewer defective tubes, requiring shortened setup time, and shortened time between tubes. It improves environmental engineering; the reduced cycle time leads to reduced, air water and hazardous waste emissions per tube. Finally, it improves product development; on-line thickness sensing is the key enabling technology to assure maximum flexibility in production capability.

The cost, energy and environment benefits listed in this proposal are for seamless steel tube and pipe only. Other savings can be realized in other parts of the steel industry. The LBU technology developed in the course of this project will have applicability to dimensional measurements in aluminum, casting, and other metal industries. For

example, the forging industry has identified development of hot-dimensional measurement capability as a top, near-term priority.[15]

References:
[1] *Steel: A Natural resource for the Future*, May 1995, pp. 1, 3.
[2] *Scenarios of US Carbon Reductions*, LBNL-40533, ORNL/CON-444, September 1997, p. 4.6
[3] *Preston Pipe and Tube Report*, 16(3), March 1998, Preston Publishing Co., (Tulsa). Used with written permission of Preston Publishing.
[4] *Scenarios of US Carbon Reductions*, LBNL-40533, ORNL/CON-444, September 1997, Figure. 4.1
[5] *Emission of Greenhouse Gases in the United States 1987-1994*, DOE/EIA-0573(94), Table A1
[6] *Scenarios of US Carbon Reductions*, LBNL-40533, ORNL/CON-444, September 1997, p. 4.27
[7] *Scenarios of US Carbon Reductions*, LBNL-40533, ORNL/CON-444, September 1997, Table 4.6
[8] *Profile of the Iron and Steel Industry*, EPA/310-R-95-005, September 1995, pp. 34-39.
[9] *The Steel Industry: A Technology Roadmap*, March 1998, p.52.
[10] *The Steel Industry: A Technology Roadmap*, March 1998, p.99.
[11] *Profile of the Iron and Steel Industry*, EPA/310-R-95-005, September 1995, p. 28.
[12] *Profile of the Iron and Steel Industry*, EPA/310-R-95-005, September 1995, p. 48.
[13] *Steel: A Natural resource for the Future*, May 1995, p. iv.
[14] *The Steel Industry: A Technology Roadmap*, March 1998, p.1.
[15] *Forging Industry Technology Roadmap*, November 1997, p. 35.

Technical Discussion of Work Performed by All Parties

• General Discussion

Timken, the world's largest manufacturer of steel seamless mechanical tubing, has for many years been interested in using an online, non-contact sensor for measuring the wall thickness and eccentricity of hot steel tubing. Methods available to date for in-process measurement of wall thickness were limited to radiation-type gauges. Such gauges do not work in the presence of a forming bar inside the tube, nor can the technique be used for small tube diameters. For some time, Timken has been interested in ultrasonics and, in particular LBU, for measuring the wall thickness of the tubing that it manufactures for various applications, particularly for bearings and gears. Their steel alloy tubing is used as feedstock for their own bearing manufacturing as well as that of their competitors. The company currently operates 4 processing lines, 3 located at the Gambrinus plant (# 3, #4 and #5 mills), Canton, Ohio and one located at the Wooster plant (#1 mill), Wooster, Ohio. The Gambrinus mills fabricate tubes ranging from 3.5" to 12" in OD whereas the Wooster mill fabricates smaller size tubing (1.5" to 4" OD). In each of the four mills, they use four operations to manufacture tubes from heated billets.

- Initial piercing: a mandrel is forced into a billet in rotation, thus making a tube.

- Elongation: the tube is pinched between three rotating rolls and is elongated with a mandrel inside it.
- Reduction: the tube (empty) is further elongated and its wall thickness reduced while passing in linear motion without rotation between several sets of pinching rolls.
- Sizing: the tube (empty) is brought to a final size while rotating between two pinching rolls.

Timken wanted to improve the control of its tube operation and for this purpose would like to have an on-line sensor for the measurement of tube wall thickness and eccentricity. A few years ago, Timken acquired a multi-head γ-ray gauge that determines tube wall thickness by tomography. This system has presented several difficulties for its implementation, for example, lack of mobility. This system also, by its principle, cannot measure tubes with a mandrel inside, i.e., during piercing and elongation. Ideally, Timken would like to have a sensor that could be easily transferred from one machine to another. Since there are four mills in operation, each including four processing operations (piercing, elongation, reduction and sizing), there are altogether 16 locations where on-line wall sensing would be of interest and could contribute to improved processing. A Timken piercing mill was used as the demonstration site for the system developed under this project.

The problem of on-line monitoring of the process of piercing steel tube is difficult. At every step in the process, the steel is orange-hot and is always moving. As it emerges from the piercing machine, the hot tube is rotating rapidly while also moving axially and vibrating severely. The environment is hostile and dirty. Any on-line sensor used to monitor this process must be capable of sustained operation in this harsh environment. Finally, anything added to the existing process must not interfere with the process, or jeopardize worker safety.

Remarkably, LBU is equal to the task. LBU uses two lasers to sense the properties of the tube as it emerges from each of the machines in the piercing process. The first acts as an optical hammer, causing ultrasonic waves to propagate in the wall of the tube. The second laser, coupled to an optical interferometer, provides a detection signal, which responds to the ultrasonic waves reverberating within the wall of the tube. By measuring the time intervals between the arrivals of these waves, wall thickness is determined after ultrasonic velocity calibration. Since lasers are used to generate and monitor the ultrasonic probing pulse, no contact is required between the sensor and the tube. Hence, the tube's motions have little consequence on the measurement process. LBU technology can achieve the high precision of conventional ultrasonic thickness gauging while eliminating the need for contact with the part.

LBU technology is based on lasers and optics, which, to some extent, are delicate and do not seem suitable for such a hostile environment. Laboratory studies have demonstrated that LBU can be hardened for industrial application. The next step in the development of LBU technology in the steel industry is to design and package the LBU elements into a system that can be used in a production environment by plant operators for long periods

of time. The unavailability of such a system, due to its development cost, has presently restricted the use of the LBU technology in the steel industry.

An international public-private partnership has been formed to apply recent advances to solve the problem of industrial implementation of LBU. The Timken Company (Timken) is the world's largest producer of steel seamless mechanical tubing. Canada's Industrial Materials Institute (IMI) is the world leader in LBU. Oak Ridge National Laboratory (ORNL) has won many awards for its developments in real-time signal processing for instrumentation.

In a 30-month project, the team combined these talents to develop a practical LBU device to perform on-line measurements during the production of steel seamless mechanical tubing. The team built and laboratory-tested a practical LBU system in the first 26 months of the project. The team demonstrated it at a Timken tube piercing plant.

Technical Approach

The wall thickness of the tube in rotation was measured with ultrasound generated and detected by lasers. The thickness of the wall at the measurement location was determined from the measurement of the time of flight between two consecutive echoes (or the initial surface pulse and the first echo) and the knowledge of the acoustic velocity. Velocity calibration as a function of temperature was obtained by heating a piece of steel of the same grade and monitoring temperature. The temperature was measured on-line by a pyrometer. More precisely since the calibration takes into account thermal expansion; one measures the thickness when the tube is at ambient temperature.

The location and timing of the laser-ultrasonic measurement is known precisely by optical velocimetry. The velocimeter was constructed using laser beams derived from the detection laser. This approach was simpler and less expensive than installation of a separate commercial velocimeter. The built-in velocimeter measures displacement along the tube axis as well as circumferential displacement. Once the tube's outside diameter is known from the precision setting of the machinery (or a laser OD gauge), the coordinates of each laser thickness measurement can be determined.

Finally, a thickness map of the tube was plotted. In particular, from this information, eccentricity will be determined at all locations along the tube length.

The configuration of the system installed and tested in the mill is shown in Figure 1. This system is modular and made of several units. Timken and IMI collaborated to develop, design, fabricate, and install this portion of the LBU. The generation and detection lasers are located remotely in a control cabin by the use of optical fibers for the generation and detection. A minimum of optical elements is located close to the hot tube and is enclosed in a front unit. This unit, located at about 5 feet from the tube, comprises coupling optics for generation, illumination for detection and collection of the scattered light, the coordinate measuring system (velocimeters optics) and the pyrometer (this unit is shown in the figure without its cover). Unlike the system tested previously at Algoma Steel by IMI and UltraOptec, which used an excimer gas laser, the generation laser is a solid state

Nd-YAG laser, which has the advantages of allowing fiber coupling and of avoiding the use of potentially dangerous gases and reducing maintenance cost. A tubular shield extends from the front unit to the probed tube to block any laser light and insures total ocular safety. The generation laser and its power supply is housed in a solid metallic cabinet. The detection laser, its power supply and the Fabry-Perot interferometer are also housed in another cabinet of the same kind. A third cabinet is used for housing all the control and processing electronics, including industrial PC computers. These cabinets are brought at the proper location by the overhead crane and are covered by a cabin provided with a door and having a configuration allowing it to be readily separated from its floor and moved at the desired location by the overhead crane. This cabin provides a barrier against dust in addition to the airtight cabinets and provides space for a system operator. Cooling of all the lasers is provided by a central industrial heat exchanger located outside the cabin. This configuration which relies on fiber coupling for generation and detection, requires only a very limited space in the immediate vicinity of the line and has the bulky equipment located far away (100 feet and even more).

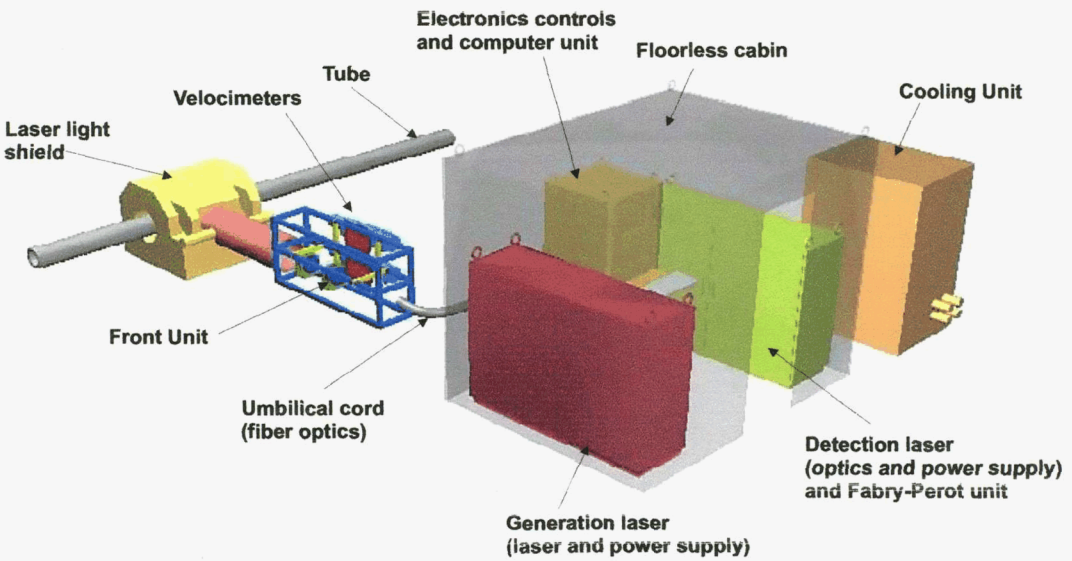

Figure 1. Schematic of the configuration of the system to be installed in the tube mill.

Advanced Signal Processing, Wireless Tube Detector, and Pattern Recognition for Product Improvement

Timken and ORNL collaborated to improve the quality of the LBU tube thickness measurement, develop a wireless tube detector, and extract tube parameters and tube dimensional patterns for process/ product improvement.

Advanced Signal Processing

There are three advantages that ORNL's recent experience in advanced signal processing that were brought to this project to enhance the performance of LBU systems:

- High-speed processing with dedicated hardware
- Wavelet analysis
- Bayesian parameter estimation

Compared to the conventional practice of analyzing the optical receiver output with the CPU of the LBU control computer, a dedicated DSP chip offers many advantages at comparatively low cost. First, there is a dramatic reduction in the volume of data flowing into the LBU CPU; for each shot of the excitation laser, the LBU CPU would see a vector of 1 to 12 numbers, as opposed to the 2800 to 3000 numbers it sees at present. Second, since the DSP chip handles the computationally costly function of feature extraction, the resources of the LBU CPU are freed up for other functions. Third, the DSP chip is fast enough to perform the feature extraction in real-time; for each shot of the excitation laser, the DSP chip will produce the output feature vector before the LBU is ready to fire the next shot. These advantages can be realized with a single DSP chip on a PCI board; this board increases the cost by $4800 for each LBU system, uses one PCI slot in the LBU control computer, and does not increase the exterior size of the system. As it turned out for this LBU system, the speed of the processor permitted the necessary calculations to complete within the sampling interval; therefore, a separate DSP baord was unnecessary. The timing was close; however, any additional cycle consuming computational tasks would require the use of the DSP subsystem.

Compared to the conventional practice of split spectrum analysis (also known as Gabor analysis), wavelet analysis is computationally more efficient. The split spectra of Gabor analysis are non-orthogonal and their outputs are overdetermined; the resulting redundant data inherently imposes inefficiencies on the analysis process. In contrast, recently discovered wavelet algorithms produce orthogonal and critically sampled output data; these data represent information with the mathematically required minimum number of data points. Although the application of wavelets to LBU signatures was investigated a decade ago, most of the dramatic advances in wavelet analysis have been made since then, and it was appropriate to revisit the topic.

Compared to the conventional practice of cross correlation with a matched filter, Bayesian parameter estimation extracts more and better information from the data in a noisy signal. Matched filtering requires *a priori* knowledge of both the model and parameters of the desired signal, and has no capability for exploiting other prior knowledge. Bayesian parameter estimation requires only the model, and then provides an estimate of the desired parameter values, and a mathematical measure of the goodness of the measure (a confidence factor). If the noisy data include the desired signal plus undesired non-random signals, Bayesian will still reliably detect the desired signal; matched filters can be confused by unexpected non-random signals. Finally, Bayesian analysis can exploit prior information to improve the goodness of the estimate.

The output of the Bayesian process enables flexibility in subsequent processes that was not previously available. The resolution of the estimated parameter values is at least an order of magnitude finer than that of conventional methods. Where conventional analysis reliably detects perhaps two pulses in the LBU receiver output, with subsequent pulses buried in the noise, it is expected that Bayesian can reliably detect one pulse more than other methods. Furthermore, instead of just the time of flight, Bayesian can provide time of flight, strength, dispersion and a confidence factor for each detected pulse. This is a wealth of information that can reveal many details of the properties of the tube being examined by the LBU system. For further details on advanced signal processing, please refer to Appendix A.

Wireless Tube Detector

The wireless system was installed in the summer of 2001and consisted of a sensor/transmitter unit, an intelligent repeater and a receiver unit that is networked to a computer. This is the first permanent installation of this system that was developed as part of DOE/OIT's crosscutting technology efforts at ORNL. This installation demonstrated the ease with which a new network could be installed in a working plant operation.

The transmitter detects the presence of a tube by optically measuring the temperature. Every 100 milliseconds, it transmits the actual value of the detector (measured volts) via a Direct Sequence Spread Spectrum (DSSS) RF link with a center frequency of 916.4 MHz. The repeater receives the message from the transmitter (at 916.4 MHz), verifies its validity, and re-transmits it via the DSSS RF link with a center frequency of 904 MHz. The receiver receives the message from the repeater at 904 MHz and processes it. Depending on the mode of operation, it sends messages to the PC and receives commands from the PC via the serial port at 38.4 Kbits/sec. The software in the control-PC relays the information to the Laser Ultra-Sonic control unit where the decision is made to turn the laser on or off. The overall goal is to extend the life of the laser tube by providing a link that allows the laser to be off when no tube is present.

This installation was the first to use the "repeater" function built into the sensor nodes. Since the process equipment blocked the direct signal path, the installation required the use of a repeater node positioned high in the room. The repeater then relayed the sensor node signals to the network node outside the building. An external antenna provided even more robustness in the connection.

When the system was first installed, we saw slight interference from a nearby nationwide pager system. Moving the center frequency of our direct sequence, spread spectrum transmitter cleared up any problems that occurred. Exposure to the harsh environments of the steel mill over the long duration of this test didn't seem to adversely effect the equipment.

Details of the overall system are in Appendix B.

Feature Extraction of Tube Parameters and Patterns

The feature extraction and pattern recognition task was a challenge technically and programmatically. Delays in the laser system startup owing to the complex nature of the instrument being developed postponed data collection for this task. Because of unexpected laser system problems, the pattern recognition task was reduced and eventually stopped so funds could be redirected to IMI to make corrections to the generation laser optics. Most of the feature extraction task could not be performed because sufficient useful data were not available.

However, even with the sparse data set collected and the work stoppage, the limited studies have provided useful information. Two items in particular are worth highlighting. First of all, although some of the more obvious patterns are visible in the raw LUT thickness graphs, bandpass filtering and/or averaging of these graphs can help isolate certain features such as low frequency thickness variations. Further study needs to be done with frequency filtering. In fact, filtering the raw data in certain frequency bands would likely help the mill operators identify certain mill conditions more easily. Second, the 2-dimensional thickness plots could be useful in helping operators discover unknown mill conditions that affect the tube as seen by the barber pole pattern in the 2-D maps.

Details of this effort including initial data and analysis are in Appendix C.

Inventions

No inventions were made or reported during this CRADA.

Commercialization Possibilities

The goal of this project was the development of an industrial LBU system for harsh environments, such as those encountered in a steel mill. Assuming that it can be made cost effective, Timken intends to use LBU to monitor the piercing process. Initially, the LBU system will profile tubing wall thickness and eccentricity. Data analysis of the LBU signal will extract features revealing many details of the manufacturing process. With this information, Timken will be able to modify the process to improve productivity and reduce waste. Ultimately, the LBU system will be used as a real-time sensor for automated process control of the piercing mill.

Several different optical system manufacturers are interested in commercial development of the technology that emerges from this research. Timken is working with these commercialization partners to transfer the technology.

Plans for Future Collaboration

A second CRADA is underway between ORNL and Timken that involves processing modeling, controls, and simulation. ORNL is providing supervisory control expertise and process optimization modeling for the entire process. Timken is providing the process models and controls for the individual unit operations.

Conclusions

The LBU system has proven to be both a complex design and a technical success. All elements of the system are working well, meeting or exceeding expectations. The initial benefits of the LBU system, reduced mill set-up time and reduced scrap, are being realized. The system has won favor of Timken manufacturing and process improvement departments.

For the majority of time since early March 2002, the LBU system has been used as a production tool, measuring more than 125,000 tubes, or nearly 75% of the tubes produced on the mill. There have been relatively minor component failures in mechanical subsystems, delivery failure in computer tracking information, and conditions that produced insufficient signal strength. It is believed that most of the factors have been eliminated and 95-98% system availability levels are readily achievable. Initial calibration studies indicated that the target accuracy of 0.5% of cold wall thickness could be met.

The wireless tube detector worked in principle but had some operational problems due to surrounding signal interference, start up delays, and data flow problems. Some of the issues were corrected but not all items were completely resolved. This is an area for potential follow on work.

The feature extraction research was initiated and some very positive resulted were generated. Unfortunately, due to project priorities and funding, this work was stopped in its early stages. This is also a potential area for future collaboration.

Appendices

• Appendix A: Program Description for Signal-To-Noise Reduction in Laser Interferometer Receiver Output Signal

WAVELET-BASED PROCESSING OF LBU THICKNESS MEASUREMENT

This is an overview of some of my results in analyzing the large data set (456 trials on the same 1" thick flat-bar sample) collected by IMI during the winter of 2000. The big concern is distinguishing between a genuine LBU pulse and a burst of noise that perversely resembles a pulse. The other concern is, supposing that we have good reason to believe that we are looking at an authentic LBU pulse, how much error does noise impose on our estimate of the time of occurrence of the pulse?

The raw data as furnished by IMI are preconditioned as follows. Setting the starting as the first sample that falls below a threshold value synchronizes all trials. Trials that failed to couple a LBU pulse into the sample were discarded. These trials were easy to identify, they fail to drive the receiver into saturation. Each of the synchronized trials is passed through a wavelet filter bank of seven levels using Daubechies 12-coefficient least asymmetric wavelet filter as the basis. All wavelet coefficients on the two scales corresponding to the 3.125-12.5 MHz band are retained, and all the others are zeroed out. These are inverse wavelet transformed with the same basis as above to recover the LBU signal with the high frequency and low-frequency artifacts removed.

Given *a priori* knowledge of the nominal sample thickness we know approximately where to look for a pulse corresponding to a particular echo. In this analysis, all algorithms take a data set of 256 samples centered on the expected location of the pulse. By using a "fixed window" (same center every time) location for all the trials, for alternative algorithms one can compare the standard deviations in the estimated time-of-occurrence (which would be zero in the absence of measurement error) and thus compare their robustness to noise.

However, on-line the tube will have eccentricity, and successive trials will have random thickness. Thus, in addition to robustness to noise, our system must be robust to the actual uncertainty in the time of flight. To simulate the uncertainty in thickness, I used a "dancing window." The center of the "dancing window" is a random variable with properties suggested by Daniel Levesque of IMI. It is Gaussian-distributed, has the same mean as the "fixed window" and a 2σ value of 70 time-bins, approximately 8% of the average time of flight of 870 time-bins between echoes. The window width is 256 samples, the same as with the "fixed window" analysis.

There are two problems that can produce misleading results. One is missing a signal that actually occurred. The other is a false call or spoof, where the system reports a signal that did not actually occur. To assess the vulnerability of the alternative methods to

misses and spoofs, the statistics for occurrences of misses and spoofs are included in the data tables. A widely accepted method of judging the believability of data is the receiver operator characteristic (ROC) curve, a plot of probability of detection versus probability of false call across a large number of trials, half with the signal present and half without. The closer the ROC curve approaches the point of 100% probability of detection and 0 probability of false call, the better the performance. By comparing ROC curves generated with the "dancing window" we can compare the vulnerability of the different algorithms to the uncertainty in location of the pulse due to eccentricity.

With luck, the same algorithms will have low standard deviations for "fixed windows" and good ROC curves for "dancing windows." Indeed this does turn out to be the case. Three algorithms outstrip all the others. One is the Blackman window, the other is the 3/6-wavelet denoiser with a Haar basis, and the other is the 23/23-wavelet denoiser with a Haar basis. For all cases, Bayesian estimation of the time-of-occurrence gave about the same performance as DFT cross correlation. The negligible improvement in estimate of time-of-occurrence does not justify the substantial added computational cost of Bayesian for this particular purpose. (However, Bayesian is handy for various other things.) The Haar basis yielded the lowest standard deviations and the best ROC curves all the different wavelet functions examined. This is remarkable, because the Haar is the computationally cheapest wavelet. A Haar filter bank can be implemented with shifts and adds, and requires no multiply operations.

Where Bayesian does come in handy is for generating the reference signal for the cross correlation. For a given echo one can obtain the Bayesian model of the pulse for each trial. If these are averaged across all trials, the parameters of the average echo can be found. This average echo is found to give consistently smaller standard deviations than result from simply picking a representative pulse from the data and using that for the reference.

One result of this analysis is that the use of the 256 time-bin sample interval is justified. It is wide enough that the pulse will trail off to approximately zero, even given the uncertainty in the time of occurrence, and the resulting end effects are negligible. Also, if the wavelet denoiser admits less than half the time-domain information, then excessively many of the authentic "dancing window" signals will be missed.

For the two wavelet-denoising algorithms the 256-element time-domain vector is Haar wavelet transformed, and in Haar space all scales are zeroed out except those corresponding to the 3.125-12.5 MHz band. Within that scale window only those samples that's time-of-occurrence is within the half of the time window in the neighborhood of the center of the time-window are retained. All the others are zeroed out. This leaves 24 non-zero samples.

For the 3/6-algorithm, all but the largest six of the remaining coefficients are zeroed out the largest non-zero coefficient is found. If two of the remaining five samples are contemporaneous, they are retained, and any non-contemporaneous samples are zeroed out. The result with only three non-zero wavelet coefficients is inverse wavelet

transformed to recover the denoised time-domain signal. This algorithm is the best of the bunch, when it works. It has the lowest standard deviations, and the best ROC curves.

In addition, if it fails, it tells you it has failed. If it cannot find the three contemporaneous pieces, it returns all zeros. The spoof rate is very low, typically two spoofs (a spoof in this case being the occurrence of three contemporaneous pieces when there should not be) in 75 trials of noise with no signal. Also, even if the spoof occurs, the cross correlation value for a spoof is much lower than that for an authentic occurrence. For excitations at 25 mJ and higher, the ROC curves are perfect. That is, if the algorithm finds the three contemporaneous pieces, and if the cross correlation value is above a comparatively low threshold, then there is 100% probability that the algorithm has captured an authentic signal.

If 3/6 is so good, why not simply use it and have done with it? While it is very robust against noise and false calls, it has an unacceptably high miss rate. For the "dancing windows" situation, it misses between 50 and 90% of authentic pulses, depending on excitation level. However, the results are so good and so cheap when it doesn't miss that it is worth using for those cases. If it tells you it has failed, then you can turn to one of the other algorithms.

For the 23/23-algorithm, the smallest of the 24 remaining coefficients is zeroed out and the other 23 are retained. The result is inverse wavelet transformed to recover the denoised time-domain signal. For "fixed window" processing through 30 mJ on the first echo, and 40 mJ on the second echo, the standard deviation performance is about the same as the Blackman window. At lower excitations the Blackman window looks better, but it only works if you have *a priori* knowledge of the location of the center of the window.

The Blackman window algorithm begins by multiplying the 256 time-domain samples by a 256 sample Blackman window. The actual window is a 3-parameter Blackman-Harris window with parameter values of 7938/18608, 9240/18608, and 1430/18608. The results for "fixed window" processing for weak excitation appear to be fairly dramatic, but it is only effective if you have a good estimate of the answer in advance. (Note: The *a priori* estimate available to the on-line instrument is not good enough, due to tube eccentricity.)

Time is found by using the discrete Fourier transform to compute cross correlation. The DFT is taken of the 256-sample list representing the signal. The DFT is taken of the time reversal of the 256-sample list representing the reference signal. The two DFTs are multiplied, and the cross correlation is recovered by taking the inverse DFT of the product. The time of occurrence of the pulse is taken as the time of occurrence of the largest absolute value of the cross correlation. This produces the time of occurrence of the phase front.

Time can also be found by assuming that the pulse is a Gaussian-windowed sinusoid, and letting the Bayesian algorithm seek the combination of frequency, window width, and time of occurrence that gives the most probable fit between the model and the data. The

result gives the time of occurrence of the group front. Since this requires a three parameter global optimization of an integral, the computational cost is high, on the order of 100 to 1000 times as many clock ticks as the DFT cross correlation.

For the "fixed window" analysis, the standard deviations in estimate of time-of-occurrence for the two time-estimation algorithms are just about the same. This leads to two conclusions. First, cross correlation should be used in the on-line system. Bayesian does not add extra value to justify its extra cost. Second, the uncertainty in time of occurrence is just about the same whether you consider the phase (cross correlation) or group (Bayesian) velocities. The effect of noise on the measurement uncertainty on the time of occurrence appears to completely overshadow the difference between group velocity and phase velocity. Thus, the assumption that group velocity equals phase velocity is a valid approximation for these data.

The ROC curves for the "dancing windows" analysis are shown below. Remember that for this case the only prior knowledge that we have is that if the pulse occurs, we expect it to occur within the wavelet processing window, but we do not know where in the window it might be, and we don't know for sure that it has actually occurred. The left column shows results for echo 1, and the right column for echo 2. The top row is the 23/23-algorithm. The bottom row is the Blackman window. The black, turquoise, magenta, blue, green, and red lines on each plot are the ROC curves for MAX, 40, 35, 30, 25, and 20 mJ excitation respectively. The horizontal axis is the probability of false call. The vertical line is the probability of detection.

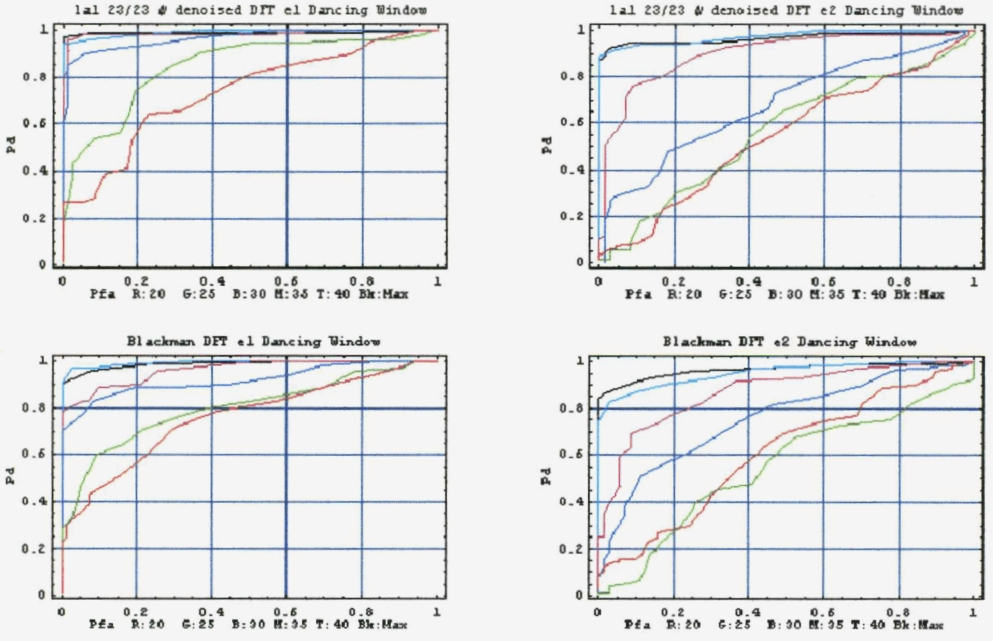

Figure 1. ROC curves for "dancing windows" 23/23 vs. Blackman

The interpretation of the ROC curves is as follows. For echo 1, and excitations of MAX or 40, the 23/23 algorithm gives >94% probability of detection with 0 probability of false call. The Blackman window is not quite as good; at these excitation levels, it gives you >91% probability of detection for 0 probability of false call. The lower excitations, the difference in performance becomes more pronounced. At 35 mJ, 23/23 gives >95% probability of detection for 2% probability of false call; Blackman gives >80% probability of detection for 2% probability of false call. At 30 mJ, 23/23 gives >86% probability of detection for 2% probability of false call; Blackman gives >72% probability of detection for 2% probability of false call. At 25 mJ, 23/23 gives >90% probability of detection for 40% probability of false call; Blackman gives >80% probability of detection for 40% probability of false call. Performance at 20 mJ is about the same for both, implying that the echo is so weak that it is usually overwhelmed by noise.

For echo 2, the comparative results are about the same. For excitations of MAX or 40, the 23/23 algorithm gives >87% probability of detection with 0 probability of false call. The Blackman window is not quite as good; at MAX and 40 mJ excitation levels, it gives you >84% and >74% probability of detection for 0 probability of false call. At 35 mJ, 23/23 gives >83% probability of detection for 20% probability of false call; Blackman gives >78% probability of detection for 20% probability of false call. At 30 mJ, on the second echo Blackman consistently outperforms 23/23. For echo 2 at 25 and 25 mJ, the curves are so intertwined and so close to diagonal that all you can say is that is that both algorithms are equally useless.

The fact that the second echo consistently shows poorer ROC curves than the first echo serves as a reality check. The overall point is that if you're looking for a pulse in the noise and you do not have prior knowledge of where in the window to look, then the 23/23-algorithm is consistently better than the Blackman window at finding the echo and not being spoofed by noise.

For the 3/6 algorithm the ROC curve has a slightly different meaning. If the algorithm fails to find three contemporaneous components in wavelet space it says, "I don't know." The only thing to do is to go to one of the other algorithms. On the other hand, suppose that it finds three contemporaneous pieces. It is probably a true call, but it may be a spoof. The ROC curve tells the story. Note that on the first echo, for all excitations greater than 20 mJ, the ROC curve is perfect. If there are three contemporaneous pieces in wavelet space, then the cross correlation is so much higher for signal than noise, that we can always tell the difference. At 20 mJ this algorithm is practically useless.

On the second echo the 3/6 algorithm gives a perfect ROC curve for MAX and 40mJ excitation. At 35 mJ the 3/6 algorithm has 90% probability of finding the second echo with 0 probability of false alarm. At excitations below 35 mJ on the second echo, the 3/6-algorithm has dubious utility.

The conclusion of the ROC curves for the "dancing window" analysis is as follows. The 3/6-algorithm is the least vulnerable to false alarms, when it works. The 23/23-algorithm

is generally less vulnerable to false calls than the Blackman window, and should be used when 3/6 tells you that it has failed. All three algorithms are reasonably robust against amount of variation in time of flight that we can expect from tube eccentricity.

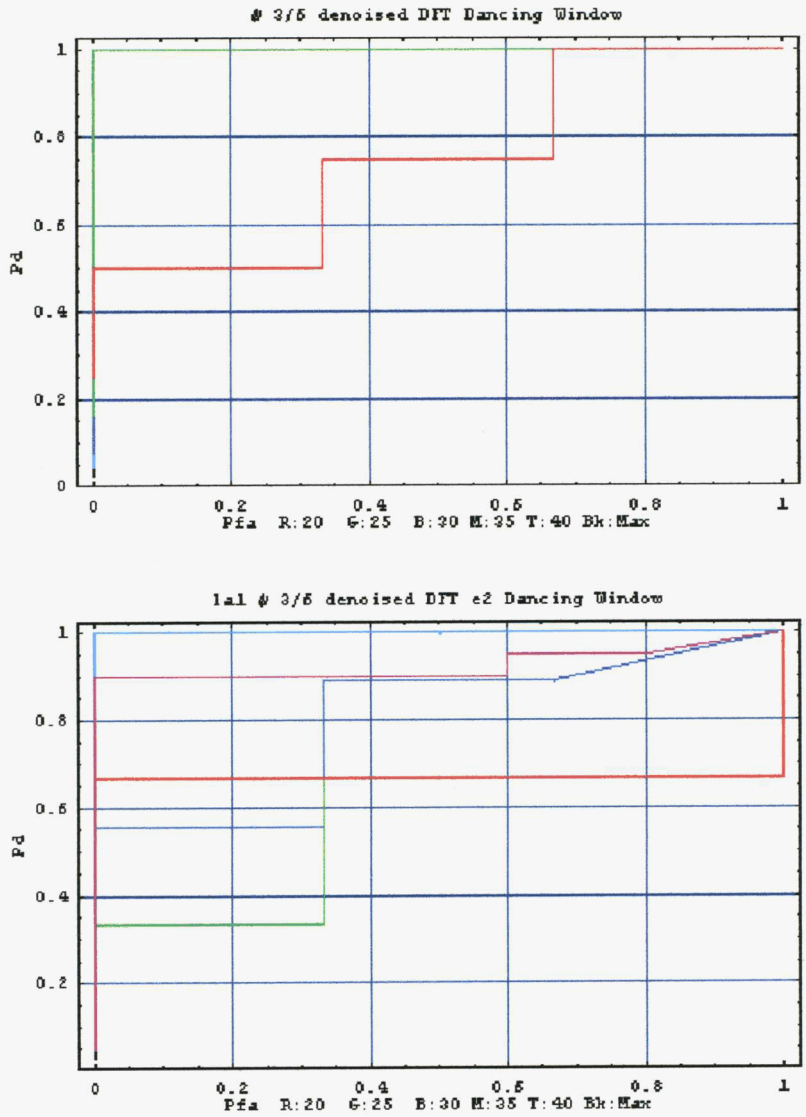

Figure 2. ROC curves for 3/6-algorithm

Tabulated data are listed below. The "Alg" column is the particular algorithm. The "mJ" column is the excitation in milliJoules. 4 σ1 is the uncertainty in the time of occurrence of echo 1. The rule of thumb is that if you do not know the distribution of random outcomes, then the safest guess is that it is Gaussian, and that for a Gaussian distribution, across many data points the most probable correct value is the mean, and any reading has 95% probability of being within 2 standard deviations of the mean. Thus, when we say that a signal has a 4 σ1 value of 1.09957 time bins, we have 95% probability that the first echo occurred within a time window 1.09957 time bins wide. 4 σ2 is the uncertainty in the time of occurrence of echo 2. ROC1 is the pair that gives the location on the ROC curve (probability of false call upper, and probability of detection lower) of the first point with a probability of detection of 90% or greater for the first echo. ROC2 is the pair that gives the location on the ROC curve (probability of false call is the upper number, and probability of detection is the lower) of the first point with a probability of detection of 90% or greater for the second echo. M1 is the number of times the algorithm completely missed the first echo when the echo actually occurred. M2 is the number of times the algorithm completely missed the second echo when the echo actually occurred. S1 is the number of times the algorithm falsely reported the first echo when no echo actually occurred. S2 is the number of times the algorithm falsely reported the second echo when no echo actually occurred.

Table 1 shows results for the 23/23-algorithm using the Bayesian algorithm to estimate time. The 23/23-denoiser always has an output. The Bayesian algorithm reports a miss whenever it is so overwhelmed by noise that the optimizer fails to converge. Table 2 shows results for the 23/23-algorithm using the DFT cross correlation algorithm to estimate time. There are no misses, but every false signal leads to a spoof. The way to distinguish the true occurrence from a spoof is by thresholding the value produced by the timing algorithm, log likelihood for Bayesian, or the computed maximum absolute value of the cross correlation.

Table 1. Results for 23/23-algorithm (Bayesian time estimation)

Alg		mJ	4 s1	4 s2	ROC1	ROC2	M1	S1	M2	S2
Dancing window la1 23 23 y denoised	Bayes	20	35.5489	34.8192	0.96 1.	0.98 0.94	25	48	16	54
Dancing window la1 23 23 y denoised	Bayes	25	33.8144	32.5465	0.66 0.9	0.88 0.93	22	59	12	58
Dancing window la1 23 23 y denoised	Bayes	30	34.9865	33.5289	0.61 0.93	0.75 0.92	17	61	18	56
Dancing window la1 23 23 y denoised	Bayes	35	34.4267	31.0471	0.46 0.91	0.76 0.9	7	63	9	54
Dancing window la1 23 23 y denoised	Bayes	40	31.0147	32.6972	0.39 0.9	0.37 0.93	19	57	14	51
Dancing window la1 23 23 y denoised	Bayes	45	29.8112	28.7861	0.15 0.92	0.15 0.92	9	59	12	60
Fixed window la1 23 23 y denoised	Bayes	20	23.7727	32.8338	0.91 0.98	0.83 0.95	26	54	14	54
Fixed window la1 23 23 y denoised	Bayes	25	20.3302	30.3065	0.86 0.91	0.98 0.95	29	59	15	59
Fixed window la1 23 23 y denoised	Bayes	30	7.90319	26.3185	0.64 0.92	0.85 0.92	21	59	18	59
Fixed window la1 23 23 y denoised	Bayes	35	2.93671	12.8404	0.53 0.9	0.81 0.91	8	62	14	62
Fixed window la1 23 23 y denoised	Bayes	40	1.59911	2.22796	0.27 0.92	0.4 0.94	5	55	5	55
Fixed window la1 23 23 y denoised	Bayes	45	1.09957	1.03269	0.03 0.92	0.07 0.99	10	61	6	61

Table 2. Results for 23/23-algorithm (DFT cross correlation time estimation)

Alg		mJ	4 S1	4 S2	ROC1	ROC2	M1	S1	M2	S2
Dancing window lal 23 23 y denoised	DFT	20	30.3444	31.2018	0.77 0.9	0.9 0.9	0	70	0	70
Dancing window lal 23 23 y denoised	DFT	25	31.9989	35.9025	0.37 0.9	0.95 0.93	0	73	0	73
Dancing window lal 23 23 y denoised	DFT	30	32.3766	29.4923	0.06 0.9	0.85 0.92	0	71	0	71
Dancing window lal 23 23 y denoised	DFT	35	28.8474	30.5005	0.01 0.92	0.34 0.93	0	71	0	71
Dancing window lal 23 23 y denoised	DFT	40	30.0373	29.0163	0. 0.91	0.01 0.9	0	70	0	70
Dancing window lal 23 23 y denoised	DFT	45	29.8294	32.2165	0. 0.91	0.01 0.91	0	75	0	75
Fixed window lal 23 23 y denoised	DFT	20	20.7741	32.6296	0.63 0.9	0.9 0.93	0	70	0	70
Fixed window lal 23 23 y denoised	DFT	25	19.5534	34.9457	0.58 0.95	0.85 0.9	0	73	0	73
Fixed window lal 23 23 y denoised	DFT	30	6.09905	24.1402	0.08 0.92	0.7 0.92	0	71	0	71
Fixed window lal 23 23 y denoised	DFT	35	1.9992	11.9414	0.01 0.94	0.25 0.96	0	71	0	71
Fixed window lal 23 23 y denoised	DFT	40	2.07738	0.739873	0. 0.94	0. 0.93	0	70	0	70
Fixed window lal 23 23 y denoised	DFT	45	0.751455	0.784535	0. 0.95	0. 0.92	0	75	0	75

Table 3. Results for Blackman window (DFT cross correlation time estimation)

Alg			mJ	4 S1	4 S2	ROC1	ROC2	M1	S1	M2	S2
Dancing window	Blackman	DFT	20	20.9164	20.7782	0.74 0.91	0.84 0.9	0	70	0	70
Dancing window	Blackman	DFT	25	27.3112	20.6193	0.78 0.96	0.95 0.9	0	73	0	73
Dancing window	Blackman	DFT	30	25.8325	19.7429	0.44 0.9	0.7 0.9	0	71	0	71
Dancing window	Blackman	DFT	35	29.298	26.2103	0.21 0.9	0.37 0.92	0	71	0	71
Dancing window	Blackman	DFT	40	32.1197	24.7309	0. 0.91	0.17 0.9	0	70	0	70
Dancing window	Blackman	DFT	45	31.8471	32.959	0. 0.91	0.11 0.92	0	75	0	75
Fixed window	Blackman	DFT	20	12.6696	17.1491	0.59 0.93	0.76 0.93	0	70	0	70
Fixed window	Blackman	DFT	25	9.35359	17.3099	0.26 0.92	0.95 0.9	0	73	0	73
Fixed window	Blackman	DFT	30	5.55919	11.5672	0.01 0.9	0.37 0.92	0	71	0	71
Fixed window	Blackman	DFT	35	2.92061	2.09589	0. 0.92	0.21 0.94	0	71	0	71
Fixed window	Blackman	DFT	40	2.37499	0.797122	0. 0.94	0. 0.91	0	70	0	70
Fixed window	Blackman	DFT	45	0.677036	0.718356	0. 0.99	0. 0.92	0	75	0	75

The results for the Blackman window are shown in Table 3. The key point is that 23/23 typically has a lower 4σ value than Blackman for the "fixed window" result. Also, as already noted, the ROC curve for "dancing windows" always looks better for 23/23 than Blackman.

The results for the 3/6-algorithm are shown in Table 4. The key point is the low spoof rate for the dancing window, regardless of excitation or timing algorithm. Although the miss rate is high, when the algorithm does not miss, it is very good, both in terms of the ROC curve for "dancing windows" and measurement uncertainty for "fixed windows."

Table 4. Results for 3/6-algorithm

Alg		mJ	4 S1	4 S2	ROC1	ROC2	M1	S1	M2	S2
Dancing window lal y 3 6 denoised	Bayes	20	26.0322	24.4916	1. 1.	1. 1.	67	2	66	4
Dancing window lal y 3 6 denoised	Bayes	25	35.8033	47.6678	Indeterminate 0.91	1. 1.	62	0	71	2
Dancing window lal y 3 6 denoised	Bayes	30	26.2584	21.9403	Indeterminate 1.	0.25 1.	55	0	63	4
Dancing window lal y 3 6 denoised	Bayes	35	23.7407	30.8921	1. 0.96	1. 0.93	47	2	57	4
Dancing window lal y 3 6 denoised	Bayes	40	34.4666	23.2724	1. 0.93	Indeterminate 0.91	43	2	48	0
Dancing window lal y 3 6 denoised	Bayes	45	29.9539	29.6065	1. 0.95	1. 0.91	36	5	43	7
Dancing window lal y 3 6 denoised	DFT	20	19.0919	13.5277	0. 1.	1. 1.	68	5	67	2
Dancing window lal y 3 6 denoised	DFT	25	47.5124	16.7432	0.67 1.	1. 1.	65	3	70	3
Dancing window lal y 3 6 denoised	DFT	30	28.5832	29.2679	0. 1.	1. 1.	62	1	62	3
Dancing window lal y 3 6 denoised	DFT	35	32.8498	34.4861	0. 0.94	0. 0.9	54	2	51	5
Dancing window lal y 3 6 denoised	DFT	40	29.7833	32.4379	0. 0.91	0. 0.94	47	5	53	2
Dancing window lal y 3 6 denoised	DFT	45	29.4054	30.4044	0. 0.94	0. 0.94	39	5	40	1
Fixed window lal y 3 6 denoised	Bayes	20	3.81952	49.142	1. 0.9	1. 1.	60	2	68	2
Fixed window lal y 3 6 denoised	Bayes	25	1.20654	23.9112	1. 1.	1. 1.	66	1	71	1
Fixed window lal y 3 6 denoised	Bayes	30	5.25821	1.63512	0.67 0.92	0.67 1.	59	3	62	3
Fixed window lal y 3 6 denoised	Bayes	35	0.67588	0.744138	1. 0.93	1. 0.9	16	1	31	1
Fixed window lal y 3 6 denoised	Bayes	40	0.558602	0.494538	1. 0.93	1. 0.9	24	2	39	2
Fixed window lal y 3 6 denoised	Bayes	45	0.669876	0.514387	0.5 0.92	0.25 0.93	25	4	45	4
Fixed window lal y 3 6 denoised	DFT	20	3.61478	48.7904	0. 0.9	0. 1.	60	2	68	2
Fixed window lal y 3 6 denoised	DFT	25	1.67616	24.0416	1. 1.	1. 1.	66	1	71	1
Fixed window lal y 3 6 denoised	DFT	30	5.75444	2.22361	0. 0.92	0. 1.	59	3	62	3
Fixed window lal y 3 6 denoised	DFT	35	0.594346	0.500641	0. 0.96	0. 0.9	15	1	31	1
Fixed window lal y 3 6 denoised	DFT	40	0.443961	0.567962	0. 0.91	0. 0.91	24	2	38	2
Fixed window lal y 3 6 denoised	DFT	45	0.631214	0.52083	0. 0.9	0. 0.9	24	4	45	4

Key comparisons of the measurement uncertainty for "fixed windows" are summarized in the following bar plots. Note that the 3/6-algorithm provides a measurement uncertainty of approximately half a time-bin width. For strong echoes, the 23/23 algorithm is just about as good as Blackman, providing a measurement uncertainty of between half and a full time-bin width. For weak echoes, Blackman appears better, but this is somewhat illusory. Blackman is using the prior knowledge of the approximate location of the pulse. The wavelet algorithms are searching in a time window 128 time-bins wide. For an eccentric tube, the instrument has no prior knowledge of the location of the pulse other than the fact that it is somewhere in the 128 time-bin window.

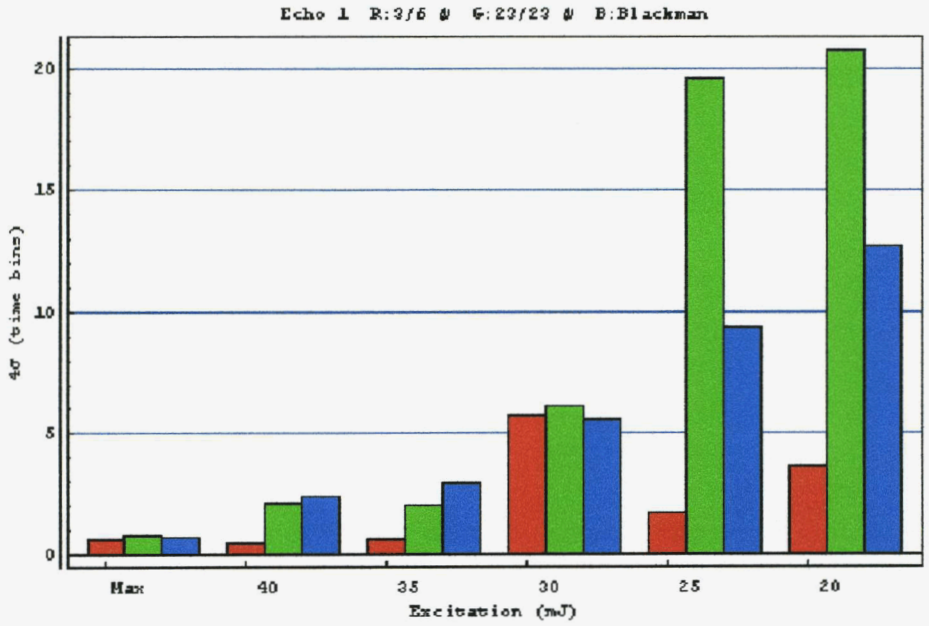

Figure 3. Comparison of measurement uncertainty - first echo all excitations

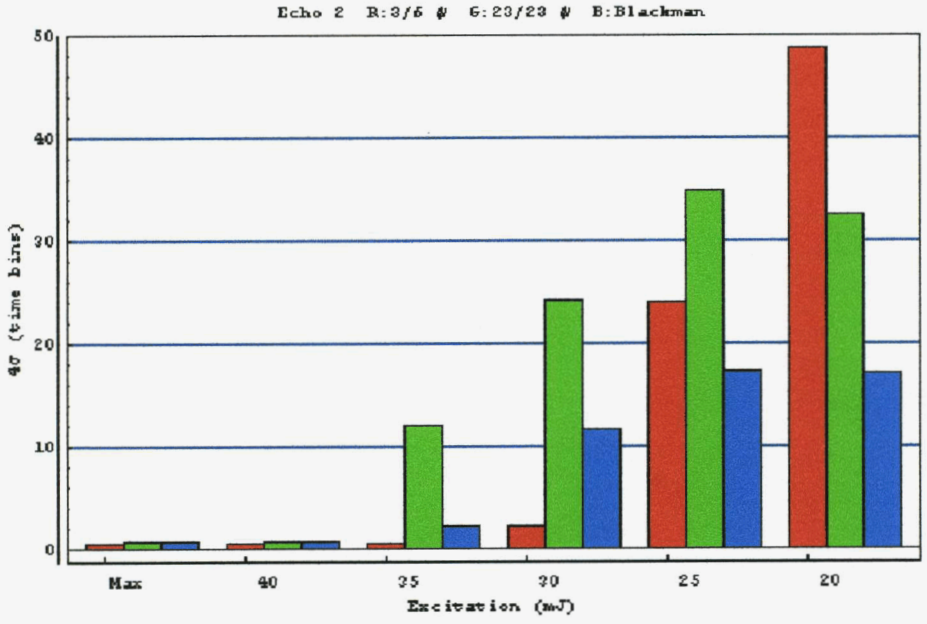

Figure 4. Comparison of measurement uncertainty - second echo all excitations

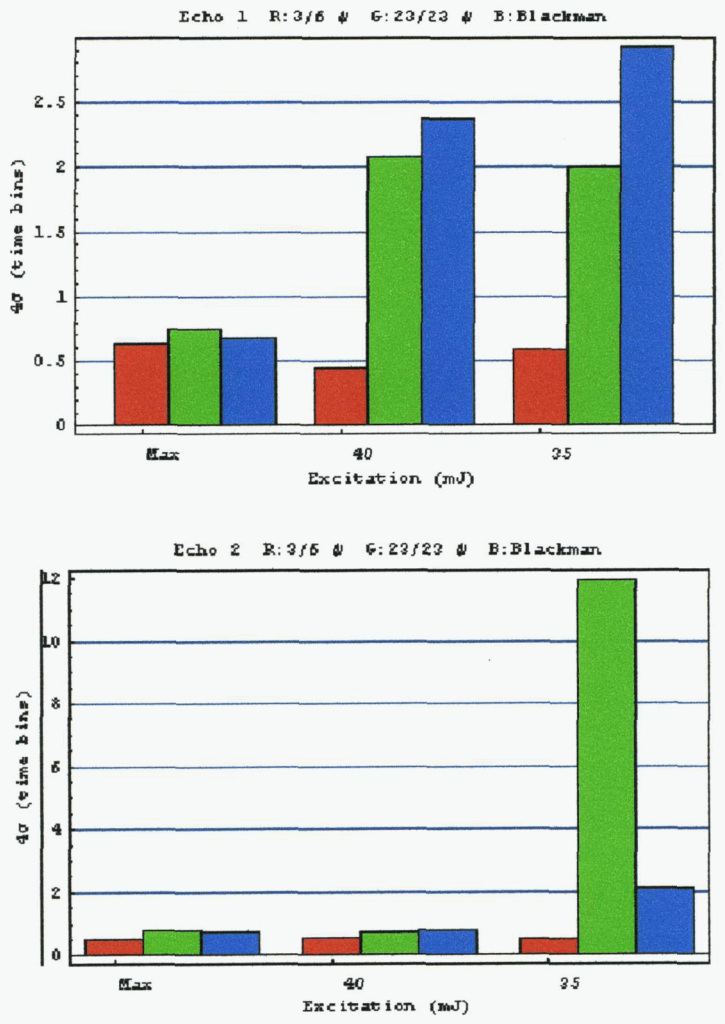

Figure 5. Comparison of measurement uncertainty – two echoes echo three excitations

Conclusions and recommendations:

The conclusion is that for this particular sample, the optimal signal processing strategy is as follows.

1) Take a 256-sample time domain vector centered on the nominal expected location of the echo.
2) Use the Haar basis to convert this vector into a 256-element discrete wavelet transform.
3) Zero out the elements at all scales except those corresponding to the 3.125-12.5 MHz band.
4) Of the 48 remaining non-zero elements, retain the 24 elements in the neighborhood of the centers of the two scales, and zero out the 24 elements near the ends.
5) Make a copy of the remaining list.
6) On the first copy of the list, zero out all but the six largest elements. Find the largest element, and check whether there are at least two more contemporaneous with it. If yes, retain the contemporaneous elements and zero out all the others, and flag this as the good list. If no, flag this as the bad list.
7) If the 3/6 list is bad, find the smallest element in the other list and zero it out. Flag this list of 23 non-zero elements as good.
8) Using the Haar basis, recover the denoised estimate of the echo by taking the inverse wavelet transform of the good list.
9) Using the DFT cross correlation algorithm with a Bayesian-derived model of the ideal pulse echo as a reference, obtain the estimate of the time-of-occurrence.

This procedure is robust for the 456 trials on a single sample. It would be desirable to check whether or not the procedure holds up for a similar number of trials for other flat bar samples, some at 1" thickness, and hopefully others at other thicknesses.

Two major things remain to be done with the existing data. One is to repeat the foregoing analysis using the Haar basis instead of the least asymmetric 12-coefficient basis in the preprocessing step. This is likely to lead to a small, but probably insignificant degradation in overall performance, but would greatly reduce the computational cost of the overall procedure.

The other remaining task is to determine whether post-processing of the cross correlation output improves the performance of the procedure. One post-processing algorithm is the time-honored split-spectrum. Another would be a wavelet-based (possibly using the fast-CWT algorithm) procedure that measures how much the cross correlation looks like the autocorrelation of the ideal reference.

Appendix A.1 Program Details

This combination of processing steps is the most effective of all the alternatives tried. It can be set to get no spoofs from noise, while simultaneously missing fewer than 10% of

good trials. There is 95% probability that the estimate of time of flight is good to within 4 time bins or fewer for excitations above 30 mJ for the first two echoes of the signal.

The first step in the C program is to query the analog-to-digital converter for a 4096-element sample list that is the data from the next trial. In other words, we should expect the raw data from the ADC written in memory as a list of integers from -2047 to 2048. Sampling rate is 100-M samples/second. Hence the sampling interval is 10 ns. We get a ringdown that dies out after about 400 samples (Fig. 6). Also note that the ringdown saturates the ADC at both extremes. We also note that the signals do not start at the same time. Following IMI's practice, we'll declare the starting point to be when the signal passes a certain threshold. Find the starting point for the signal. Signal starts with the first element whose value is below the threshold.

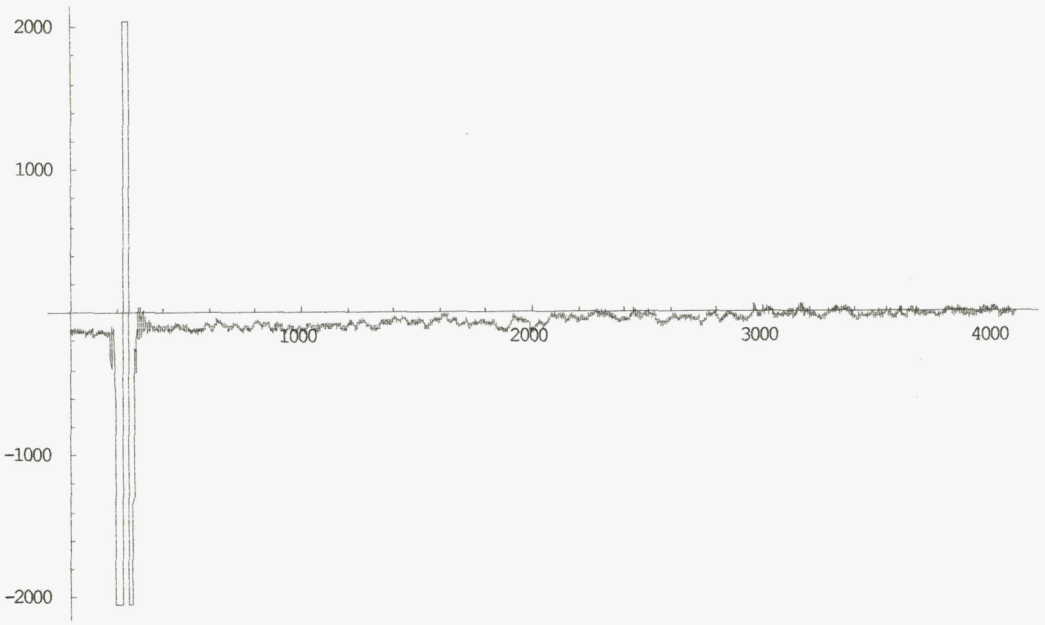

Figure 6. Typical Raw Signal

Occasionally you get misfires; the laser fires, but no signal is excited. These must be detected. Find the misfires. Each trigger event must be tested to check if the ultrasonic signal formed. If yes, continue. If no, the trial returns no data. If it is true that the maximum value in the list is less than the top rail or if the minimum value in the list is greater than the bottom rail, then it is true you have a misfire, and the analysis of this vector is complete. If the proposition evaluates to false, then you do have saturation levels.

If the saturation lasts for less than 30 time bins, then the ultrasonic signal probably does not form. The saturation pattern is that the signal bottoms out then tops out. The software checks the time of occurrence of the last top rail value, and the time of occurrence of the

first bottom rail value. If it is true that the difference is less than 30, you have a misfire. If the proposition evaluates to false, then assume the signal is good.

Both of the foregoing propositions must evaluate to false if the laser firing results in a good signal. After a good signal is captured, the DC bias is subtracted out.

The initial stage of processing is by wavelet screening. A six-level filter bank using Daubechies least-asymmetric 12-coefficient filter is used. The effect of screening out the two finest wavelet levels and the three coarsest levels is that bandpass filtering is obtained. Everything below 3.125 MHz and above 12.5 MHz is filtered out. This assures that the receive laser noise is filtered out, and that high frequency noise will not be aliased by decimation to change the sampling rate.

In addition, the wavelet denoising algorithms provide time-pass filtering. They use a window of 256 time-bins-wide centered about the expected time of occurrence of the echo. Within that window, we can center our space-time 128 time-bins-wide window wherever it is needed. Everything outside the 128 time-bins-wide window is zeroed out. The denoising window is periodic. The space-time window wraps around if it is specified near the edge.

The signal is transformed into the wavelet domain. After signal outside the desired time-pass/bandpass window is zeroed out. The zeroed out version in inverse wavelet transformed to recover the time-domain signal.

The next step is Donoho denoising. The time-domain signal is Haar wavelet transformed. In the Haar-domain all but the 24 samples in time-pass/bandpass region are zeroed out. Of these 224 samples, the one sample with the smallest absolute value is zeroed out. The Haar-domain signal is inverse transformed to recover the denoised time-domain signal.

An ideal exemplar for each echo was determined by Bayesian parameter estimation on signals collected under controlled conditions. Time of flight is determined by split spectrum processing combined with cross-correlation. The DFT of the denoised time-domain signal is taken. The DFT of the exemplar is taken. The DFT of the Gabor basis function is taken. These are multiplied together. The product is inverse DF transformed to obtain a cross correlation of the three signals. The process is repeated at uniformly spaced Gabor frequencies throughout the range of 3-18 MHz. The result is a list of split spectrum signals.

The feature vector has two components. The split spectrum signal with minimum entropy is the one with the best developed peak. The difference in the earliest and latest maximum time of occurrence of the cross-correlation peak as we sweep across the Gabor scales is the other feature. A small number means the peak is not moving much with Gabor frequency, and indicate a coherent signal. A big number suggests noise. For each signal figure the distance of its time of occurrence from the average time of occurrence across the entire Gabor domain. The feature vector for each of the split spectrum signals is the distance of the peak time of occurrence from the average time of occurrence, and

the the entropy. The two features are only weakly correlated implying that they contain non-overlapping information.

The cluster centers in feature space were computed for multiple samples with a strong echo and no echo. Compute the mahalanobis distance of the each split spectrum signal signal from the good cluster less the mahalanobis distance of the signal from the bad cluster. Select the signal with the shortest Mahalanobis distance to the center of the good cluster. If it is closer to the bad cluster than the bad cluster
reject it as noise. If it is not noise, its time of occurrence gives the time of occurrence of the signal.

This combination of processing steps is the most effective of all the alternatives tried. It can be set to get no spoofs from noise, while simultaneously missing fewer than 10% of good trials. There is 95% probability that the estimate of time of flight is good to within 4 time bins or fewer for excitations above 30 mJ for the first two echoes of the signal.

Table 1. Typical Test Results (Echo 1)

Excitation (mJ)	Valid Firings	95% Probability Resolution Time Bins	Good Trials Ignored as Noise
20	70	66.12239038429247	16
25	73	48.54841535910087	12
30	70	8.217302558820908	8
35	72	3.3374890258977525	1
40	71	3.04337178163336	1
Max	75	3.0825285046503597	0

The ROC curve (Fig. 7) indicates the tradeoff between probability of detection and probability of false call. The ROC curve shown in Figure 2 shows that the algorithm is very robust against errors for excitations above at 35 mJ and above, tolerable at 30 mJ and unacceptable below 30 mJ. The vertical axis is probability of detection of good signal. The horizontal axis is probability of false alarm (confusing noise burst with signal).

Figure 7. ROC Curve

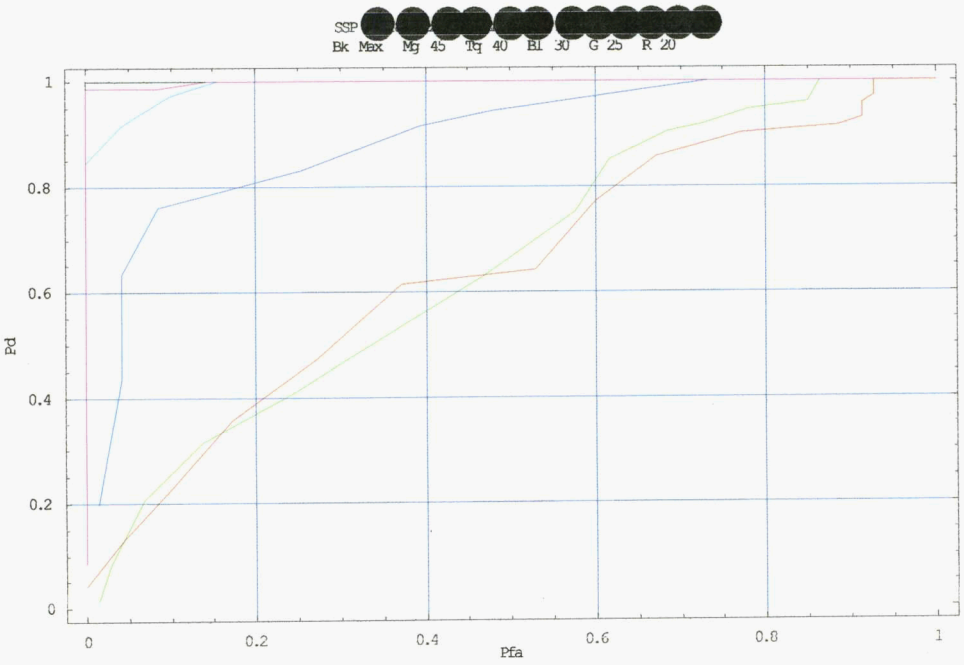

********************** Program Description **********************

amain_LBU.cpp - Defines the entry point for the console application.

This is the set of functions needed for the implementation of the signal processing
algorithm for the Timken Laser ultrasonic thickness measurement system.

Developed by

Stephen W. Kercel

Brian Damiano

Roger A Kisner

Oak Ridge National Laboratory

January 30, 2001

Function of program: